An assessment of structural enthalpy and crystallization pathways of $Mg_{65}Zn_{30}Ca_5$ bulk metallic glass and amorphous films

Scott Gleason, David Miskovic, Nicholas Hamilton, Kevin Laws, Michael Ferry

UNSW Australia
School of Material Science and Engineering

August 10, 2017

ABSTRACT

The structural nature and thermal stability of amorphous alloys is highly dependent on the method by which they are produced, i.e. their relaxation rate upon cooling. Both bulk samples and metallic glass films of $Mg_{65}Zn_{30}Ca_5$ were produced by copper mold casting and direct current (DC) magnetron sputtering onto aluminium substrates, respectively. Comparisons between structural enthalpy, crystallization pathways, relaxation and crystallization kinetics of the bulk samples and films were examined by elevated temperature XRD and DSC. Compared with equivalent experiments on the bulk alloy, results for the thin films show distinct differences in structural enthalpy and deviations from the expected crystalline phase evolution, displaying minor peak shifts, failure of some phases to evolve, and variations in the evolution rates.

TABLE OF CONTENTS

1 INTRODUCTION

The structural nature and thermal stability of amorphous alloys is highly dependent on the method by which they are produced, i.e. their relaxation rate upon cooling. Both bulk samples and metallic glass films of $Mg_{65}Zn_{30}Ca_5$ were produced by copper mold casting and direct current (DC) magnetron sputtering onto aluminium substrates, respectively. Comparisons between structural enthalpy, crystallization pathways, relaxation and crystallization kinetics of the bulk samples and films were examined by elevated temperature XRD and DSC. Compared with equivalent experiments on the bulk alloy, results for the thin films show distinct differences in structural enthalpy and deviations from the expected crystalline phase evolution, displaying minor peak shifts, failure of some phases to evolve, and variations in the evolution rates.

2 METHOD

2.1 Master alloy

The master alloy of $Mg_{65}Zn_{30}Ca_5$ was produced using high-purity elements of Mg (99.85 wt%), Zn (99.995 wt%), and Ca (99.8 wt%). The alloy was prepared by induction melting in boron nitride coated graphite crucibles, purged with Ar (99.997 vol.% purity) five times, and protected with a circulating Ar atmosphere. Alloy homogeneity was ensured by heating and cooling through a cycle of 700°C, 385°C, 650°C, 385°C, 650°C to a casting temperature of 500 °C and 450°C for injection and gravity casting respectively. Bulk amorphous $Mg_{65}Zn_{30}Ca_5$ rods of 2.5mm diameter and plates of thickness of $XX\mu m$ were produced by copper mold injection casting. The 25.4mm diameter targets were prepared from a cylindrical copper mold gravity castings sectioned to thicknesses of 3.25mm. All samples and targets were stored under Ar when not being examined or used.

2.2 DC magnetron sputtering

Films were produced from an in-house DC magnetron sputtering facility with Ar working gas (99.997 vol.% purity). The power was 15W, typical voltage of $290 - 350V$, nominal chamber pressure of 1 bar, substrate temperature of 25°C, and Ar flow of 3.01 SCCM. Films were deposited directly onto to Al DSC lid substrates. Depositions were for a period of 35 minutes. Deposition rate was estimated at 1.2nm/s.

2.3 Stylus profiler analysis

Nominal film thickness was measure by a stylus profiler (Dektak 2A, Bruker, Germany). A glass slide was placed under the substrates within the sputtering chamber, allowing the substrates to act as a mask. Profile measurements were taken by measuring the height difference between the bare glass and the film coated glass. This film thickness was used to estimate the sputter deposition rate.

2.4 EDS analysis

Alloy composition and homogeneity were confirmed by SEM-EDS (S3400, Hitachi, ?Japan?). Hyper-maps were collected with a accelerating voltage of $15 - 20kV$, and a probe current of $50\mu A$. (Conditions; counts were 5000 kps or better, dead time was less than 20 %, and working distance was 10mm).

2.5 DSC characterization

Isochronic DSC (204 F1 Phoenix, Netzsch, Selb, Germany) was carried out in Al crucibles under a protective Ar atmosphere (99.997 vol.% purity). Scans were performed at heating rates (βs) of 5 to $100K/min$.

Isothermal relaxation DSC was preformed by heating samples at $20K/min$ to the desired annealing temperature, holding for desired time, and Ar quenching to room temperature.

For annealed XRD the samples were heat treated in the DSC by heating to the desired temperature at $20K/min$ followed by Ar quenching to room temperature.

2.6 XRD characterization

Annealing XRD (Empyrean, PANalytical, Cu K_α X-ray source, $\lambda = 1.541$Å) was performed at room temperature. (Generator Voltage 45, Tube Current 40, Scan Step Size 0.0262606, Time per Step 397.29).

Dynamic XRD (D8, Bruker, Cu K_α X-ray source, $\lambda = 1.541$Å) was performed by raising temperature at a rate of $20K/min$ and performing scans *in situ*. The first scan was performed at 35°C, then 75°C, after which temperature was raised in $5K$ increments until reaching the peak temperature at 185°C. The 2θ scans from $31 - 60^\circ$ were completed within $1092sec$

(18min, 12sec) to minimise the effects of recrystallisation during the experiment. (Generator Voltage 45, Tube Current 100, Scan Step Size 0.02, Time per Step 134.4).

3 RESULTS

3.1 Alloy composition

From the 35 minute depositions a nominal film thickness of 2.5μm was obtained, giving a deposition rate of approximately 1.2nm/s. The temperature within the chamber was found to rise $3-4$°C, significantly less than the expected 20K suggested by similar setups [1].

EDS analysis shows good agreement in the nominal composition for both the bulk and film $Mg_{65}Zn_{30}Ca_5$, see Table 1.

EDS Analysis	Bulk (at%)	Film (at%)
Mg	64.85 ± 3.18	62.92 ± 3.24
Zn	29.55 ± 0.82	31.17 ± 0.95
Ca	5.60 ± 0.17	5.91 ± 0.19

Table 1: EDS composition of bulk and film $Mg_{65}Zn_{30}Ca_5$ in atomic weight percent.

3.2 DSC

3.2.1 Isochronic DSC

Isochronic DSC was performed on the bulk and film $Mg_{65}Zn_{30}Ca_5$ to examine the thermal properties. The bulk alloy was relaxed at 120°C for 10 minutes before DSC measurements to ensure the T_g was clearly visible. The film was not relaxed as unlike the bulk the lost in free volume from relaxation would be significant and make differences between the samples much more difficult to observe [source needed???].

The bulk $Mg_{65}Zn_{30}Ca_5$ was examined at heating rates (βs) of 5, 10, 15, 20, 30, 40, 60, 80, and 100 K/min to observe changes in the T_g and the T_xs with β. As expected greater β resulted in greater signal strength, exothermic peaks shifting to higher start temperatures, and an increase in thermal lag resulting in later exothermic finish temperatures and curve convolution. With this convolution the T_g and T_{x1} remained clearly visible for all βs, but $T_{x2,4,5}$ were only visible at low βs, and T_{x3} was not clear at any β, see Figure 1.

The film was examined at βs of 15, 20, 30, 40, 60, 80, and 100 K/min. The lower βs of 5 and 10 k/min were not utilised owing to the lower film signal compared to the bulk. The reduced signal was likely from the low mass of the film, about $\frac{1}{10}$ that of the bulk. The film showed the expected variable relationships with increasing β as observed in the bulk. The signal intensity increased at a compatible rate to bulk up until βs of 80 and 100 k/min. These final two βs showed great increases in the signal intensity. The exothermic peaks all convoluted together making many of the thermodynamic events difficult to observer. It also appeared that all exothermic events shifted to lower temperatures as compared to the bulk. The T_g and T_{x1}s were less defined than for the bulk, but could still be identified for all βs. For all βs the T_{x2-5} onsets could not be easily identified, see Figure 2.

3.2.2 Fragility

Using the isochronic DSC data the fragility (m) of the $Mg_{65}Zn_{30}Ca_5$ system could be established for both the bulk and film. Numerical solutions where used to fit the DSC variant of the Vogel–Fulcher–Tammann (VFT) relationship for β [2].

$$\beta^{-1} = \tau_0 \, e^{(\frac{D^* T_0}{T_g - T_0})} \tag{1}$$

Where τ_0 is a pre-exponential factor, D^* is the liquid fragility parameter, and T_0 is the VFT temperature where the barrier to flow becomes infinite.

The m could then be calculated from Equation 2 [3, 4].

$$D^* = 590/(m - 16) \tag{2}$$

Using these two equations for the bulk it was found $\beta^{-1} = 1.338E - 16e^{5274(\frac{1}{T-T_0})}$ with an Adj. $R^2 = 0.972$. This gave a $D^* = 20.4$, and a m= 44.9. The film was fitted to $\beta^{-1} = 5.921E - 11e^{2766(\frac{1}{T-T_0})}$ with a lower confidence of Adj. $R^2 = 0.861$, likely owing to the reduced number of data points. This gave a $D^* = 10.0$, and m= 75.0, see Figure 3.

3.3 DSC deconvolution

3.3.1 Onset determination

Numerical solutions were used to deconvolute the isochronic DSC data so the various T_x onsets could be accurately determined. This numerical fitting utilised a summation of skewed Gaussian curves to fit a target curve corresponding to the original data; as is a common method [5–9]. This fitting summation takes the form of Equation 3 .

this is n
a place

$$f(x) = \sum_{n=i}^{n} h_i \, e^{-} \left(\frac{(x - T_i)^2}{(2c_j)^2} \right) \tag{3}$$

Where h is the enthalpy peak intensity, T is the temperature at the enthalpy peak centre, and c is the Gaussian RMS width.

The final converged solutions of this fitting for both the bulk and film are shown in Figures 4 and 5 respectively. These results are tabulated in Table 2 for the bulk and Table 3 for the film. Note T_g and T_{x1} are obtained from the original raw data, not the deconvolution.

It is worth noting the deconvolution fitted 5 crystallisation events for the bulk $Mg_{65}Zn_{30}Ca_5$, but only 3 events for the film. This occured because the bulk had 5 well defined events, where as the film was largely convoluted together. Thus unique solutions could not be obtained by the lesser T_{x2} and T_{x4} events of the film.

Heating Rate β K/min	T_g	T_{x1}	T_{x2}	T_{x3}	T_{x4}	T_{x5}
100	136.1	164.8	193.4	201.8	240.2	262.4
80	132.0	160.0	194.4	201.9	238.2	260.3
60	129.6	157.7	190.0	197.8	232.9	259.0
40	126.6	155.2	189.0	200.0	226.4	254.7
30	126.2	151.5	187.0	198.4	221.0	251.1
20	125.1	149.8	188.4	197.0	216.0	246.8
15	123.8	148.3	186.2	195.6	212.2	243.9
10	123.5	144.5	183.4	192.9	207.4	239.8
5	120.5	141.1	179.7	187.5	199.8	232.7

Table 2: Bulk $Mg_{65}Zn_{30}Ca_5$ alloy onset temperatures for the various DSC heating rates β. All temperatures are in $^{\circ}$C.

Heating Rate β K/min	T_g	T_{x1}	T_{x2}	T_{x3}	T_{x4}	T_{x5}
100	108.5	128.6		177.3		240.3
80	106.0	121.2		165.6		238.8
60	107.3	134.0		176.1		237.8
40	100.2	119.8		170.7		234.2
30	95.3	110.4		169.5		232.5
20	95.5	115.2		170.5		229.4
15	92.5	113.5		168.8		224.0

Table 3: Film $Mg_{65}Zn_{30}Ca_5$ alloy onset temperatures for the various DSC heating rates β. All temperatures are in °C.

3.3.2 Reaction enthalpy

The deconvolution fits were integrated to find the area under each curves. This information provides the specific enthalpy (h) of the crystallization of each phase. This is presented in Tables 4 and 5 for the bulk and film respectively. Figure 8 shows the T_x onsets and specific enthalpy (h) for both the bulk and film plotted together.

Heating Rate β K/min	$h_{T_{x1}}$ J/g	$h_{T_{x2}}$ J/g	$h_{T_{x3}}$ J/g	$h_{T_{x4}}$ J/g	$h_{T_{x5}}$ J/g
100	59.59	6.97	49.16	22.84	46.08
80	42.61	6.08	32.33	18.27	31.25
60	30.02	4.05	25.41	16.76	19.81
40	16.93	4.36	12.44	11.13	11.68
30	12.03	3.68	9.32	9.18	9.02
20	7.18	2.21	4.99	5.67	5.78
15	5.48	2.01	3.65	4.69	4.43
10	3.45	1.43	2.28	3.14	2.92
5	1.65	0.69	1.09	1.47	1.42

Table 4: Bulk $Mg_{65}Zn_{30}Ca_5$ alloy h of crystallisation for Tx_{1-5} for the various DSC heating rates β; h is in J/g.

3.3.3 Relaxation enthalpy

For next paper on relaxation / rejuvenation.

Heating Rate β K/min	$h_{T_{x1}}$ J/g	$h_{T_{x2}}$ J/g	$h_{T_{x3}}$ J/g	$h_{T_{x4}}$ J/g	$h_{T_{x5}}$ J/g
100	48.24		49.85		43.38
80	43.27		53.56		36.18
60	15.5		8.78		22.4
40	16.22		9.13		16.27
30	13.72		7.16		11.81
20	6.16		2.3		7.45
15	6.99		3.66		6.57

Table 5: Film $Mg_{65}Zn_{30}Ca_5$ alloy h of crystallisation for Tx_{1-5} for the various DSC heating rates β; h is in J/g.

3.4 XRD

3.4.1 Annealing XRD

The crystallisation events observed and deconvoluted from the DSC were further examined with annealing XRD. Both the bulk and films were heat treated by annealing to 120, 140, 145, 170, 200, 250, 290, and 320°C before XRD. This allowed for the location of the T_g and T_xs to be confirmed as well as for the crystallisation phases to be identify.

From these experiments 5 previously observed crystallisation phases of the MgZnCa system [10–14] were characterised in the bulk and film $Mg_{65}Zn_{30}Ca_5$. This allowed the crystallization process of $Mg_{65}Zn_{30}Ca_5$ from the fully amorphous glass to fully crystalline metal to be identified as;

$$\text{Glass} \rightarrow Mg_{51}Zn_{20} \rightarrow Mg \rightarrow Ca_2Mg_5Zn_5 \rightarrow MgZn \rightarrow Ca_2Mg_5Zn_{13}$$

The annealing XRD results are shown in Figures 9 and 10 for the bulk and film respectively. In these figures each phase is identified with a tracer at the temperature it was most strongly observed. Note the Al substrates peaks have been faceted in Figure 10 as to not dwarf the other peaks.

In Figures 9 and 10 it can be observed that $Mg_{51}Zn_{20}$ comes out at lower temperature in the film compared to the bulk, while the other phase nucleate and grow at similar rates for both the bulk and film. The temperature each phase is first and last observed are tabulated in Table 6.

3.4.2 Dynamic XRD

The annealing XRD was useful for identifying the crystal phases present, but not many difference between the evolution rates of the bulk or films could be observed. Thus samples

Phase	Bulk		Film	
	First Temp	Last Temp	First Temp	Last Temp
Glass	35	200	35	200
$Mg_{51}Zn_{20}$ [10, 13]	170	200	140	200
Mg	170	320	140	320
$Ca_2Mg_5Zn_5$ [10, 14]	200	250	200	250
MgZn [13]	250	250	250	250
$Ca_2Mg_5Zn_{13}$ [10–12]	290	320	290	320

Table 6: Temperatures at which each crystallisation phase is first observed and last observed in the annealing XRD for both the bulk and film. All temperatures are in °C.

were subjected to dynamic XRD over their most active rang to observe changes *in-situ*. This allowed the crystallisation to be watched live for seeing how phase evolved over time as the temperature was raised in 5 °C increments.

4 DISCUSSION

The use of a 60K DSC heating rate compared to the more commonly used 20K rate [sources] shifts peaks for the bulk $Mg_{65}Zn_{30}Ca_5$ alloy about 8 - 15 degrees higher. This higher heating rates were used because crystallization events for the films were difficult to differentiation at the lower heating rate. Films show little shift to high temperature peaks with increases heating rates, but large shifts with relaxation. Bulk show the opposite behaviour, larger peaks shifts with higher heating rates and little shift with relaxation.

5 CONCLUSIONS

6 ACKNOWLEDGEMENTS

Yu Wang for his assistance with XRD experimentation and Rietveld refinement.

7 REFERENCES

[1] J. Q. Wang, N. Chen, P. Liu, Z. Wang, D. V. Louzguine-Luzgin, M. W. Chen, and J. H. Perepezko. The ultrastable kinetic behavior of an Au-based nanoglass. *Acta Materialia*, 79(0):30–36, 2014.

[2] R. Busch, W. Liu, and W. L. Johnson. Thermodynamics and kinetics of the Mg65Cu25Y10 bulk metallic glass forming liquid. *Journal of Applied Physics*, 83(8):4134–4141, 1998.

[3] C. A. Angell and S. Borick. Specific heats Cp, Cv, Cconf and energy landscapes of glassforming liquids. *Journal of Non-Crystalline Solids*, 307 - 310:393–406, 2002.

[4] Shuai Wei, Zach Evenson, Isabella Gallino, and Ralf Busch. The impact of fragility on the calorimetric glass transition in bulk metallic glasses. *Intermetallics*, 55:138–144, 2014.

[5] Samir K. Ashour and Mahmood A. Abdel-hameed. Approximate skew normal distribution. *Journal of Advanced Research*, 1(4):341–350, 2010.

[6] Yuzo Yamamoto, Yuichi Inoue, Teruaki Onai, Chikashi Doshu, Hiroshi Takahashi, and Hiroki Uehara. Deconvolution analyses of differential scanning calorimetry profiles of β-crystallized polypropylenes with synchronized x-ray measurements. *Macromolecules*, 40(8):2745–2750, 2007.

[7] Charles H. Spink. *Differential Scanning Calorimetry*, volume Volume 84, pages 115–141. Academic Press, 2008.

[8] Charles H. Spink. The deconvolution of differential scanning calorimetry unfolding transitions. *Methods*, 76:78–86, 2015.

[9] Balázs Schäffer, Béla Schäffer, and D. Lõrinczy. Decomposition of dsc curves of dairy products with gaussian functions. *Journal of Thermal Analysis and Calorimetry*, 82(2):531–535, 2005.

[10] Y. N. Zhang, G. J. Rocher, B. Briccoli, D. Kevorkov, X. B. Liu, Z. Altounian, and M. Medraj. Crystallization characteristics of the Mg-rich metallic glasses in the Ca-Mg-Zn system. *Journal of Alloys and Compounds*, 552:88–97, 2013.

[11] Yi-Nan Zhang, Dmytro Kevorkov, Xue Dong Liu, Florent Bridier, Patrice Chartrand, and Mamoun Medraj. Homogeneity range and crystal structure of the Ca2Mg5Zn13 compound. *Journal of Alloys and Compounds*, 523:75–82, 2012.

[12] Yi-Nan Zhang, Dmytro Kevorkov, Florent Bridier, and Mamoun Medraj. Experimental study of the Ca-Mg-Zn system using diffusion couples and key alloys. *Science and Technology of Advanced Materials*, 12(2):025003, 2011.

[13] Y. Khan. Dynamic temperature crystallization behaviour of amorphous and liquid Mg70Zn30 alloy. *Journal of Materials Science*, 24(3):963–973, 1989.

[14] Jake D. Cao, Thomas Weber, Robin Schäublin, and Jörg F. Löffler. Equilibrium ternary intermetallic phase in the Mg-Zn-Ca system. *Journal of Materials Research*, 31(14):2147–2155, 2016.

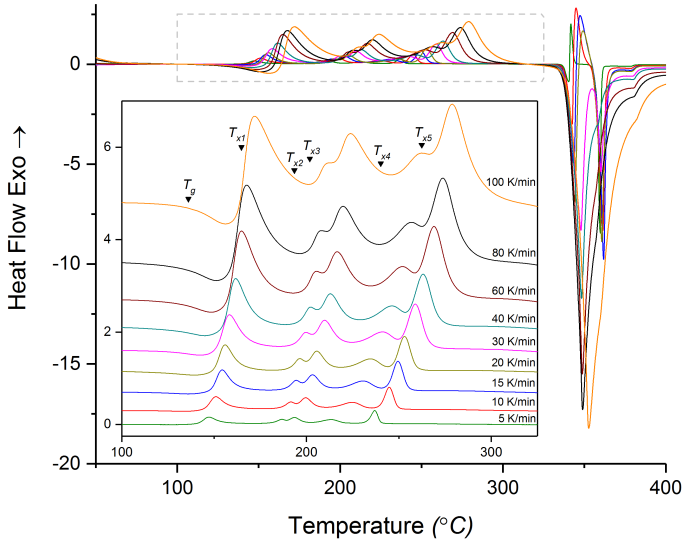

Figure 1: Bulk $Mg_{65}Zn_{30}Ca_5$ relaxed at 120 °C for 10 minutes and heated at various heating rates (βs) from 5 to $100K/min$. The insert stacks the differential scanning calorimetry (DSC) curves and labels the T_g and T_xs of the $\beta = 100K/min$ sample.

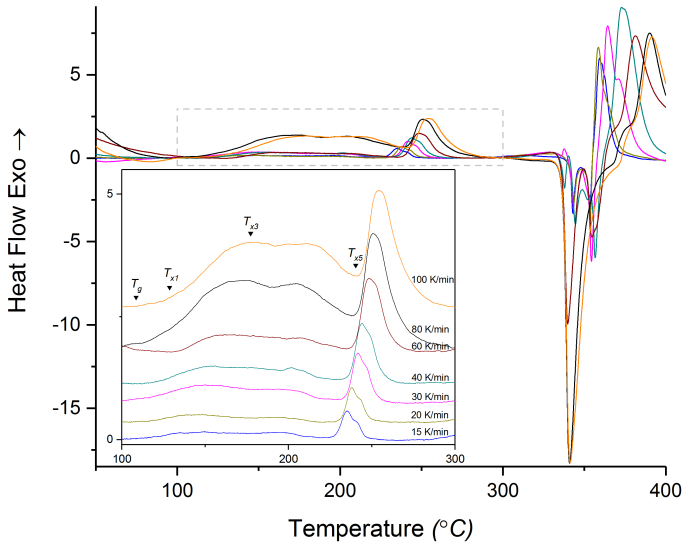

Figure 2: Unrelaxed film $Mg_{65}Zn_{30}Ca_5$ heated at various heating rates (βs) from 15 to $100K/min$. The insert stacks the DSC curves and labels the T_g and T_xs of the $\beta = 100K/min$ sample.

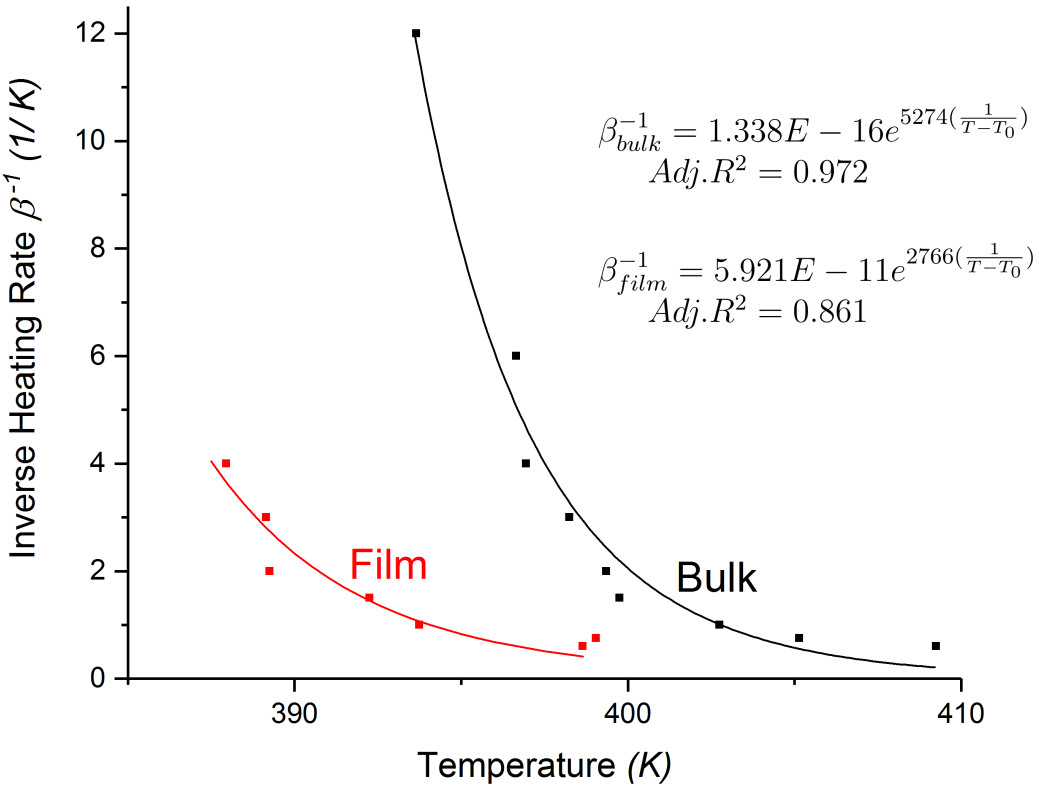

Figure 3: Fitted fragility (m) for the $Mg_{65}Zn_{30}Ca_5$ system obtained from the T_g of DSC at various heating rates (βs) for the bulk and film.

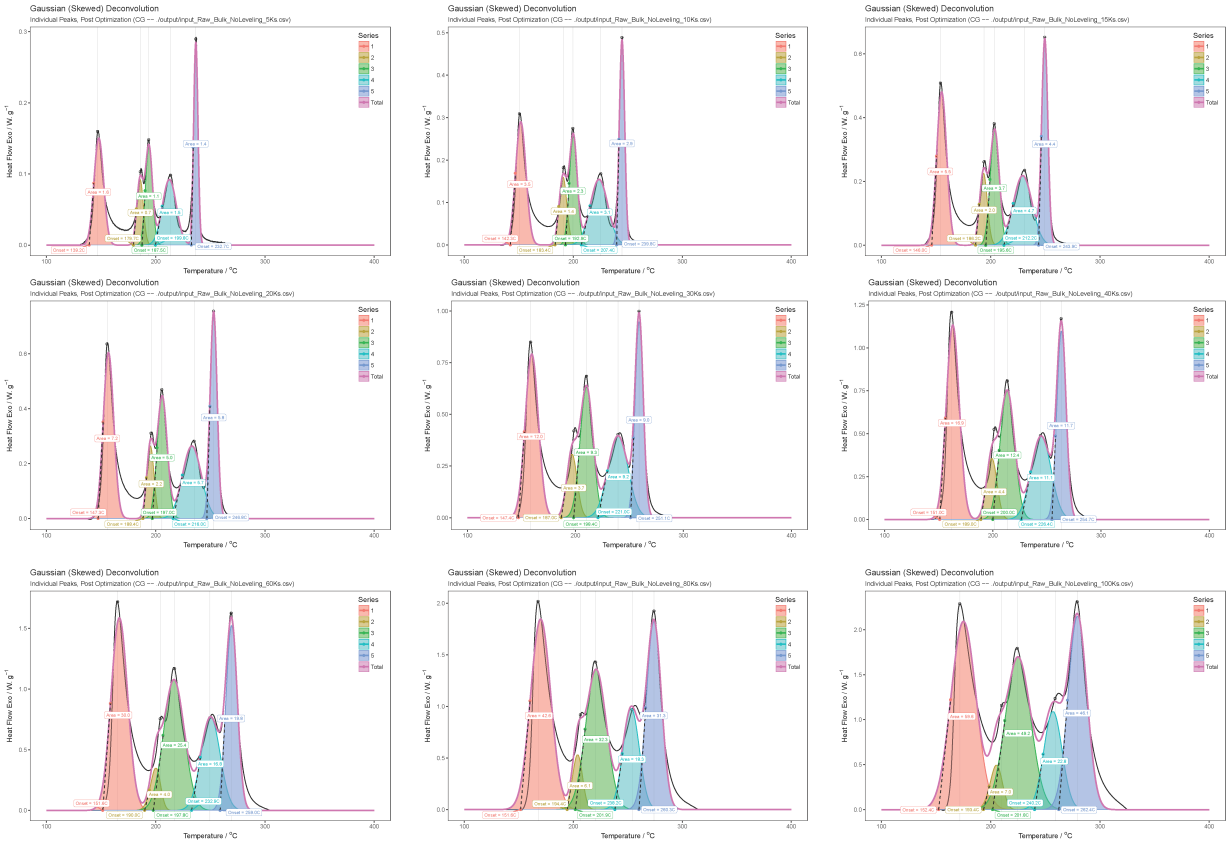

Figure 4: DSC deconvolution for the bulk at various heating rates (βs). From left to right, top to bottom, β = 5, 10, 15, 20, 30, 40, 60, 80, 100 K/min.

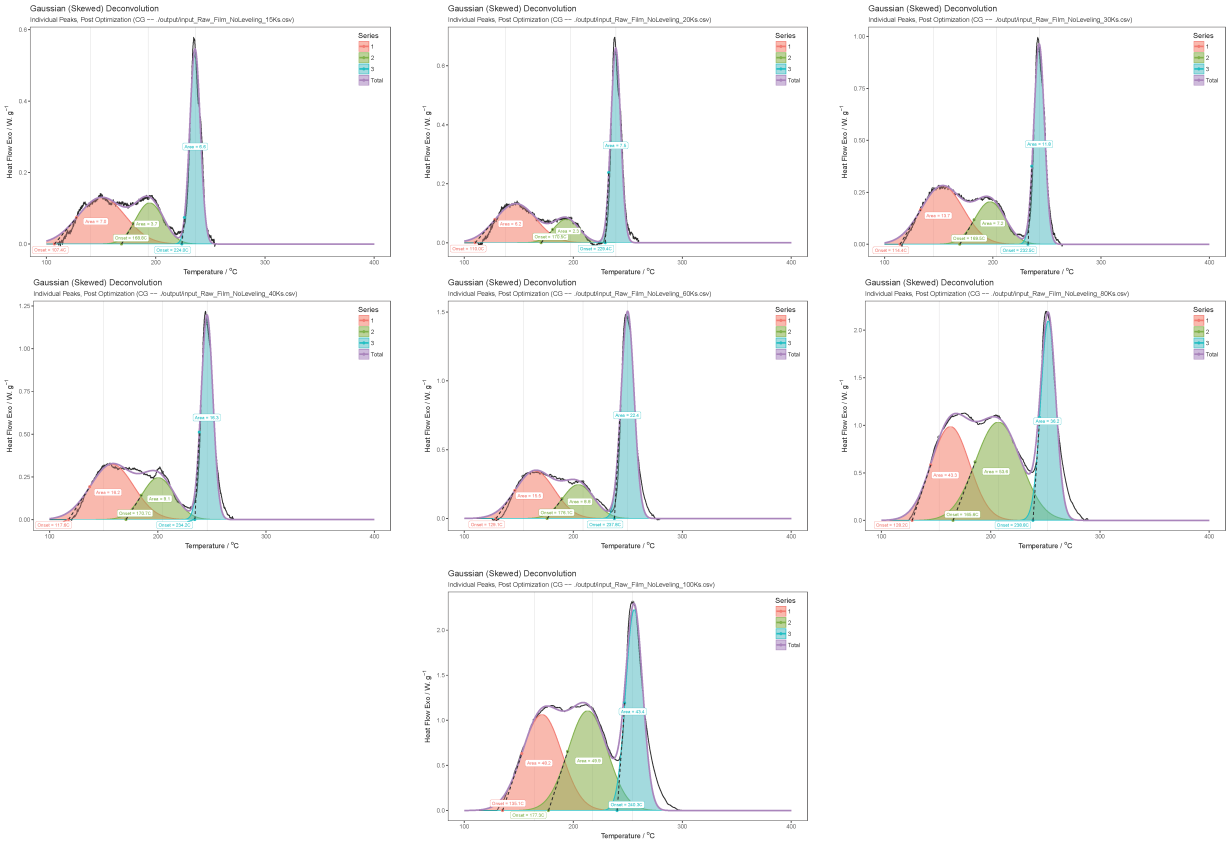

Figure 5: DSC deconvolution for the film at various heating rates (βs). From left to right, top to bottom, β = 15, 20, 30, 40, 60, 80, 100 K/min.

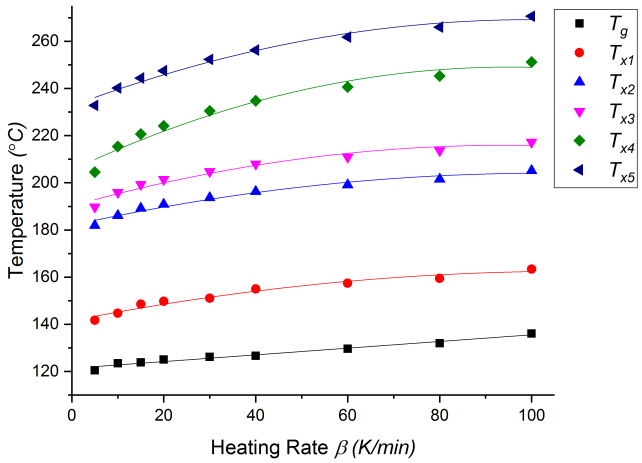

Figure 6: The T_gs and T_xs plotted at each DSC heating rate (β) for the bulk $Mg_{65}Zn_{30}Ca_5$.

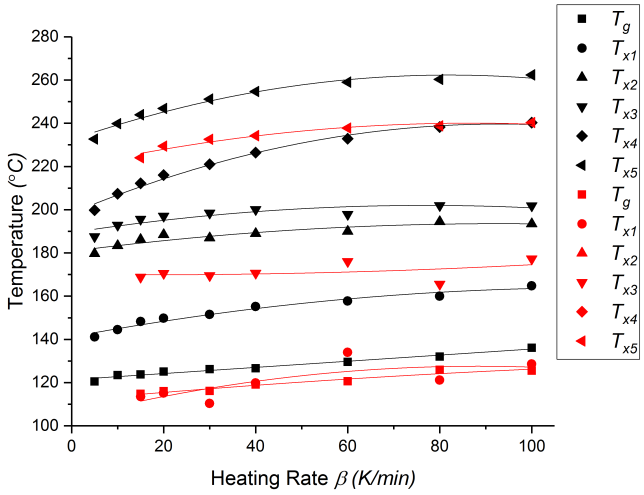

Figure 7: The T_gs and T_xs plotted at each DSC heating rate (β) for both the bulk and film $Mg_{65}Zn_{30}Ca_5$. Bulk is shown in black, and film in red.

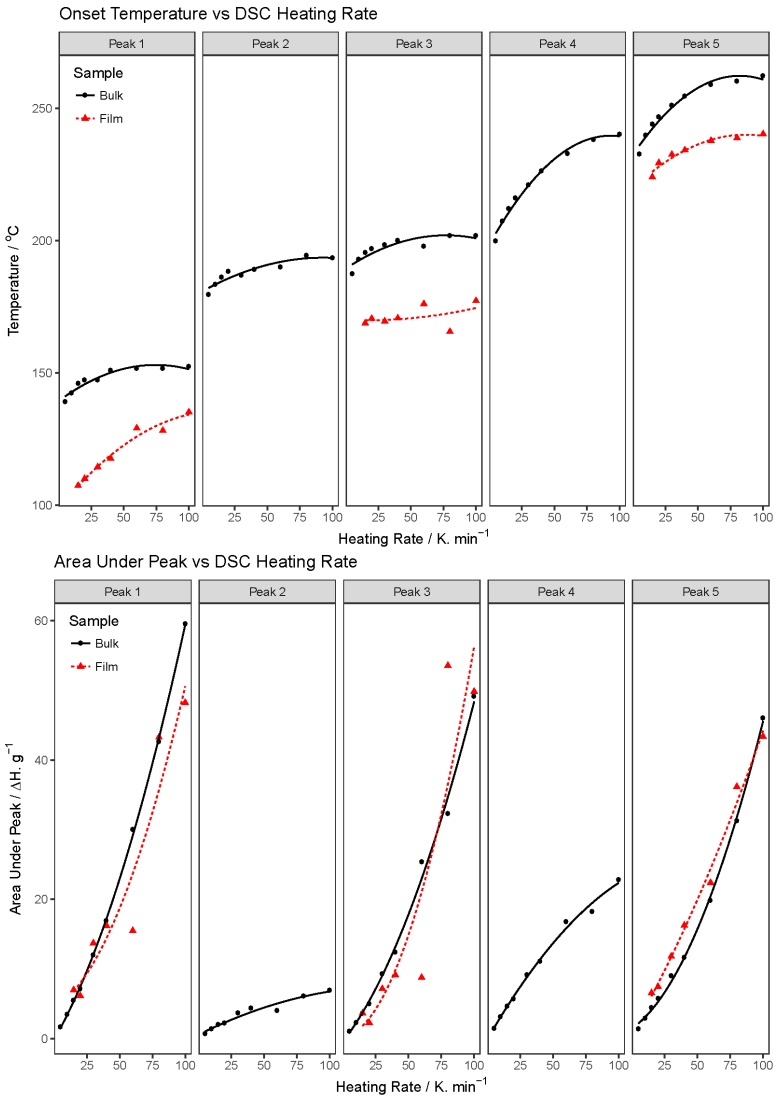

Figure 8: DSC T_x onset temperatures and specific enthalpy (h) of crystallisation formation for the bulk and film at each heating rate (β). Bulk is shown in black, and film in red.

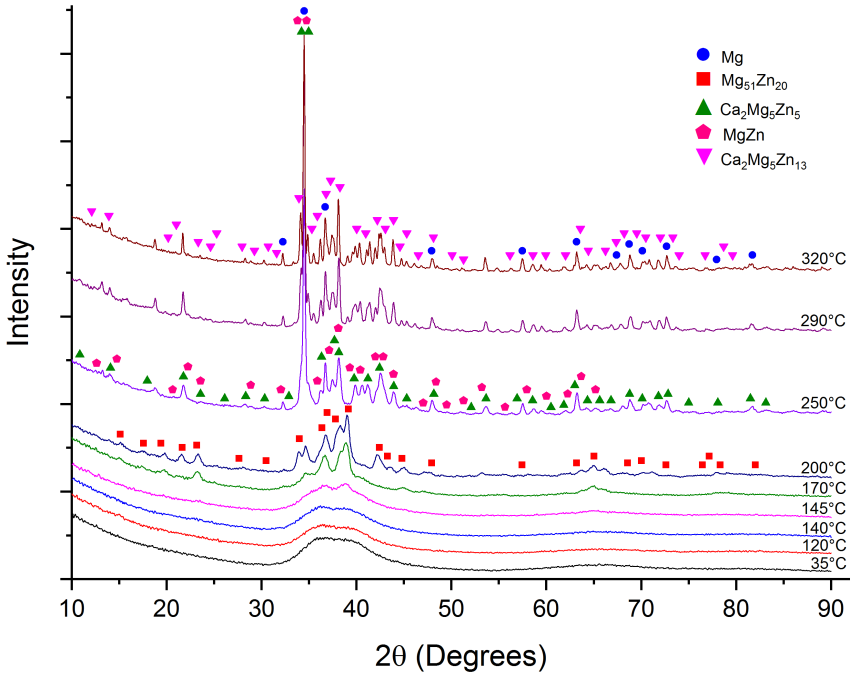

Figure 9: XRD pattern for bulk $Mg_{65}Zn_{30}Ca_5$ heated treated to several temperatures for crystallization peak identified from DSC.

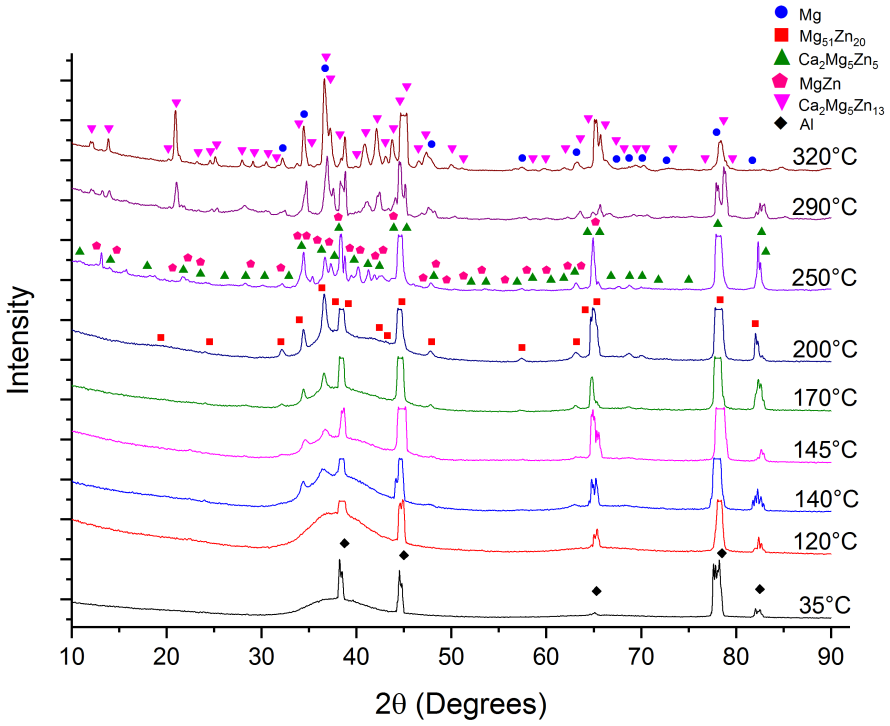

Figure 10: XRD pattern for film $Mg_{65}Zn_{30}Ca_5$ heated treated to several temperatures for crystallization peak identified from DSC. Note the Al substrate peaks have been faceted as to not dwarf all other peaks.

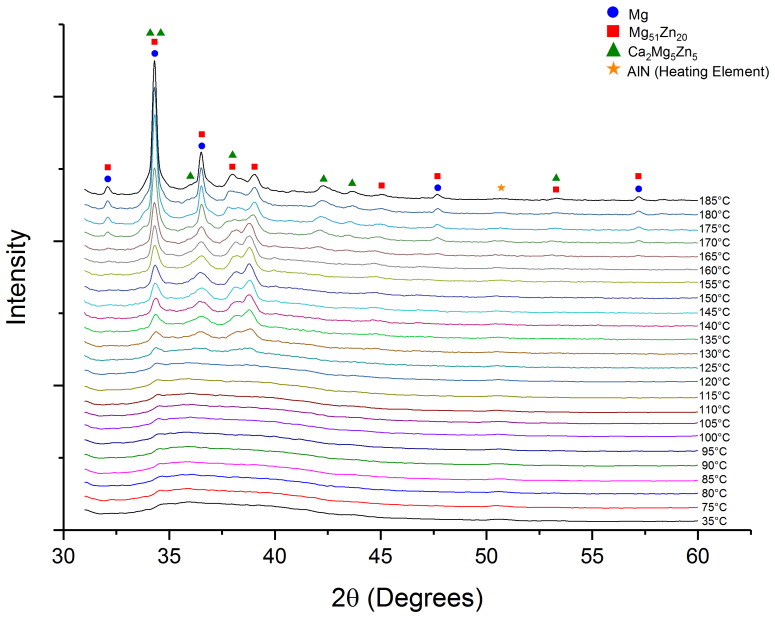

(a)

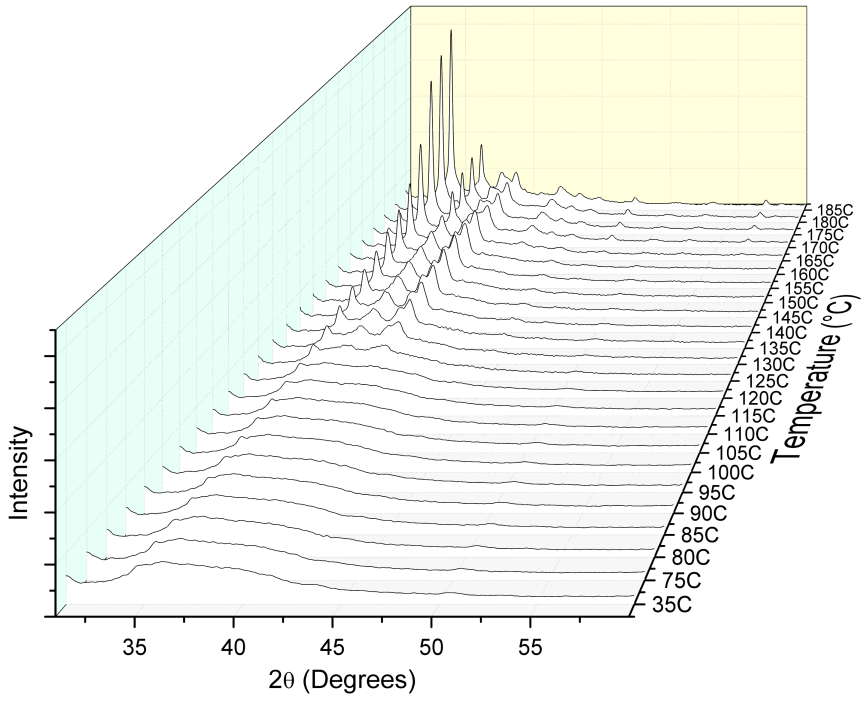

(b)

Figure 11: (a) Stacked XRD patterns from the incremental dynamic *in-situ* heating of bulk $Mg_{65}Zn_{30}Ca_5$. Note the peak around 51° is attributed to the AlN heating element. (b) The same XRD patterns as (a) presented in a cascading layout.

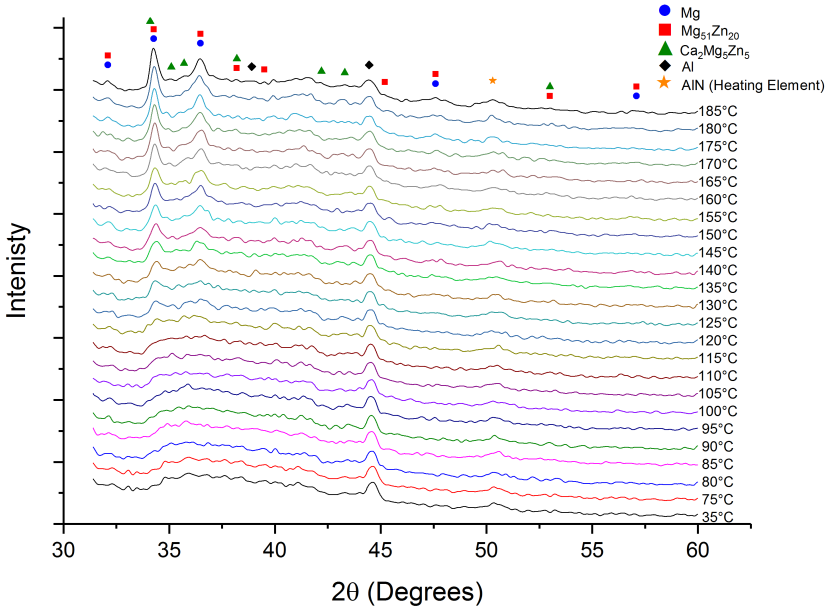

(a)

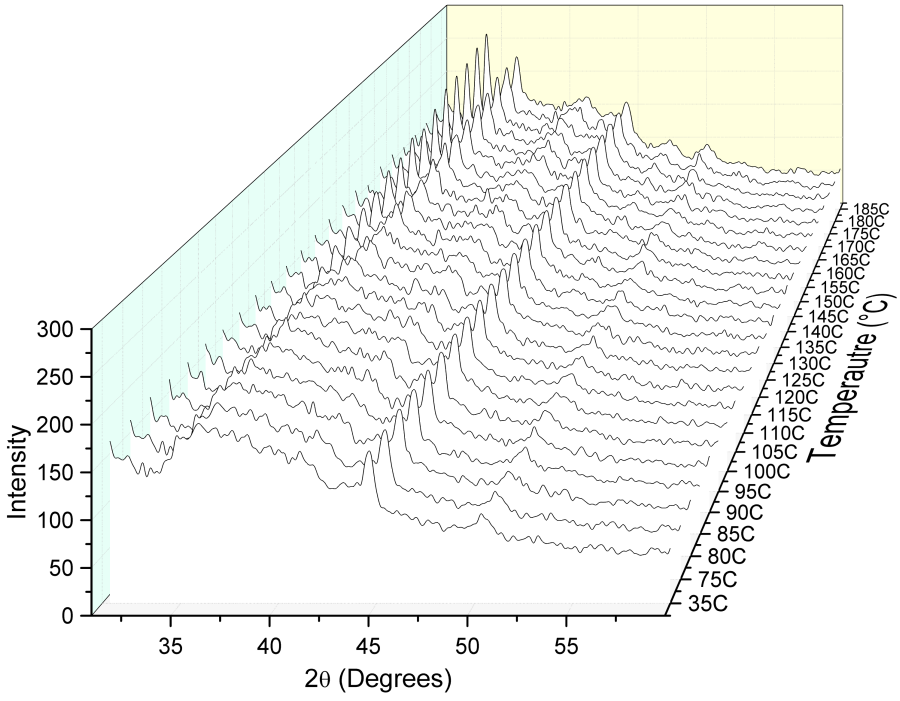

(b)

Figure 12: (a) Stacked XRD patterns from the incremental dynamic *in-situ* heating of film $Mg_{65}Zn_{30}Ca_5$. Note the peak around 51° is attributed to the AlN heating element, and the Al substrate peaks have been faceted as to not dwarf all other peaks. (b) The same XRD patterns as (a) presented in a cascading layout.